Electric Potential Profile with Distributed Degradation in the Terminal Joint for ITER TF Coil System

Shin HASEGAWA, Hideki KAJITANI, Yasuhiro UNO, Tsutomu KAWASAKI, Mio NAKAMOTO and Masataka NAKAHIRA

National Institutes for Quantum Science and Technology, Naka 311-0193, Japan

ITER toroidal field coils are electrically connected to 68-kA main busbars (terminal joints). We propose the measurement of the electric potential distribution in a terminal joint using electrical probes (e-probe method) to inspect the contact resistance in the joint. In this study, we experimented with a mockup of a terminal joint. The test current was 20 A, and the electric potential was measured using the e-probe method at room temperature and 77 K. Nine different degradation patterns were prepared by distributing polyimide films in the joint interface. Next, we performed finite element analysis to investigate the detailed relationship between the electric potential distribution and contact resistance at 300 K and 77 K. In the numerical analysis, the same degradation patterns and test current as in the experiment were assumed. The analysis results agree with the experimental results. Different degradation patterns exhibit different electric potential profiles with 10-μV-scale differences. The analysis results also indicate that the e-probe method works when the contact resistance in the degraded area is larger than 1.0×10^{-5} Ωmm^2 at 77 K and 300 K.

© 2024 The Japan Society of Plasma Science and Nuclear Fusion Research

1. Introduction

An ITER toroidal coil (TFC) is electrically connected to the 68-kA main busbar of a feeder (terminal joint), as shown in Fig. 1 [1, 2]. A large electrical contact resistance leads to severe consequences, such as magnet quenching and arc discharge. Thus, confirmation of the local increase in the contact resistance due to joint degradation is necessary, and it is desirable to perform it at room temperature (RT) during the TFC-feeder assembly.

In addition, the contact resistance in the TFC double pancake joint (DPJ) was inspected during winding pack (WP) manufacturing [3, 4]. The electric potential distribution along the DPJ was measured using electrical
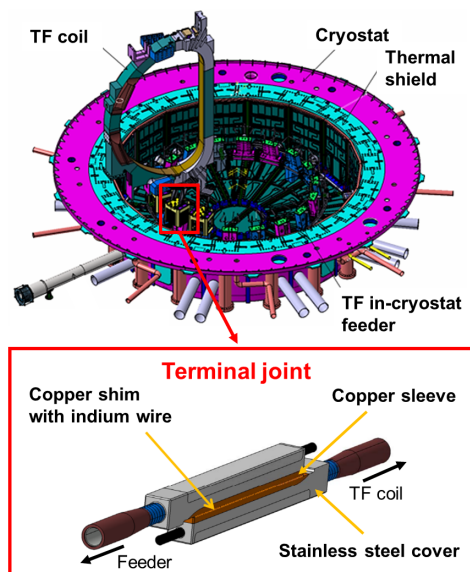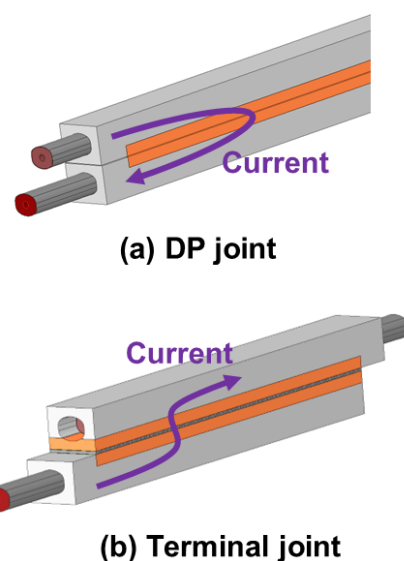

Fig. 1　Terminal joint for the ITER TF coil system.

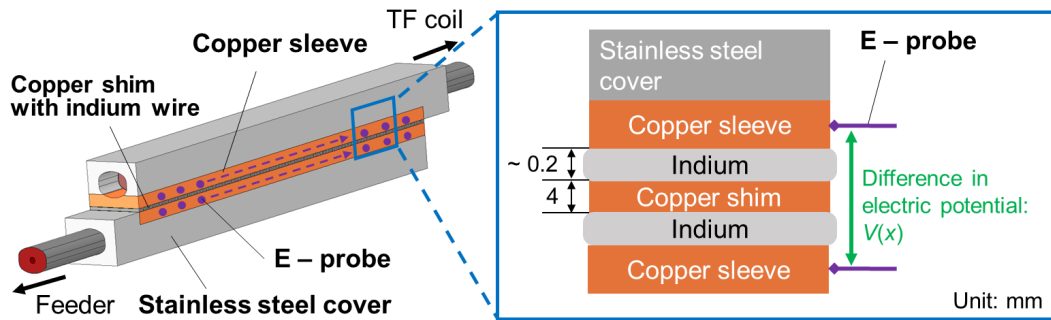Fig. 2　Different current path in (a) DPJ [3] and (b) terminal joint.

Fig. 3 E-probe method for the terminal joint where electrical probes are distributed on the copper sleeve of the terminal joint.

probes (e-probes) when a test current was applied (e-probe method). This method was implemented for all WPs of Japanese TFCs. Although the structure of the DPJ differs from that of the terminal joint, the materials and electrical characteristics of the jointed superconducting conductors are almost the same. Thus, we propose the use of the e-probe method for the inspection of the terminal joint.

The difference between the structures of the terminal joint and the DPJ may lead to a difference in the current path and electric potential distribution, as shown in Fig. 2. Thus, in this study, we first experimentally investigated the electric potential distribution in the terminal joint using the e-probe method with a mockup of the joint. As a first step of this investigation, we focus on the degradation (large contact resistance), which is easily detected to understand the characteristics of the electric potential distribution and limitations of the e-probe method. The degradation assumed in this study is uniform in the width direction and distributed in the longitudinal direction. This degradation possibly occurs because of the imbalanced compression of the joint during the TFC-feeder assembly. The experiment was conducted at RT and 77 K to improve the sensitivity of the electric potential distribution to the degradation distribution. The relationship between the value of contact resistance in the degraded area and the electric potential distribution is important for understanding the limitations of the e-probe method. However, it is difficult to precisely control the value of the contact resistance in the experiment. Thus, a numerical analysis was performed assuming a wide-range contact resistance, its distribution, and different operating temperatures (RT and 77 K).

Section 2 explains the e-probe method for the terminal joint. Sections 3 and 4 present the methodology of the experiment and numerical analysis, respectively. Section 5 presents the results and discussion, followed by a conclusion in Sec. 6.

2. E-Probe Method for Terminal Joint

Figure 3 shows the structure of the terminal joint and a conceptual diagram of the e-probe method. Two superconducting conductors are joined by a copper shim and an indium foil. The contact resistance in superconducting conductors is already known during their manufacturing. Therefore, the resistance between the two copper sleeves of the superconducting conductors should be measured. In the e-probe method, electrical probes are attached to the side surface of the copper sleeve of each conductor along the longitudinal direction, and a test current is applied. Then, the electric potential difference between the two copper sleeves is measured along the longitudinal direction. First, we should obtain the measurement or simulated data for the terminal joint without any degradation. Using these data as a reference, an increase in the contact resistance can be identified.

3. Experiment

An experiment was conducted by preparing a mockup of the actual size of the terminal joint. Figure 4 shows a mockup of the terminal joint. The two joint box samples [3–5], which primarily comprise superconducting cables, stainless steel covers, and copper sleeves, were joined with indium wires and a copper shim. The superconductor used for the TFC winding and joint box sample was Nb_3Sn, whereas that for the main busbar was made of Nb-Ti. This study aimed to confirm the characteristics of the electric potential distribution in the joint. The influential parameter that differs between Nb-Ti and Nb_3Sn is electrical resistivity. This difference is only 6% - 9% at 77 K - 300 K [6, 7]. Thus, this is considered to be a negligible difference in this study. The assembly procedure of the mockup was as follows: 1) indium wires with a diameter of 1.2 mm were wound on the copper shim; 2) one joint box sample was placed; 3) the copper shim with the indium wires was placed on the copper sleeve of the superconducting conductor; 4) stainless steel shims with a thickness of 0.2 mm were placed on the copper shim to make the thickness of indium 0.2 mm) another joint box was placed on the copper shim. Polyimide sheets were inserted between the copper shim and sleeve instead of the indium wire to represent an increase in the contact resistance (degradation). The region of the joint interface with a length of 588 mm was divided into two (Zones A1 and A2) or three (Zones
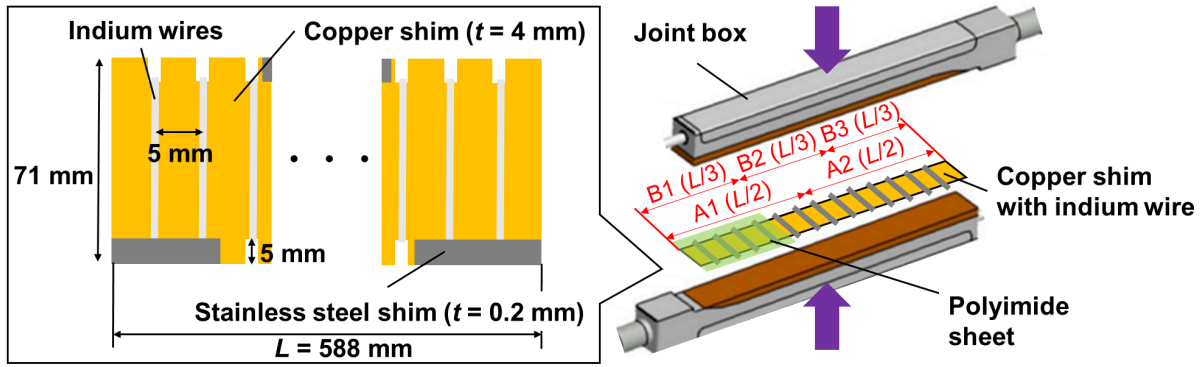
Fig. 4   Assembly procedure of the mockup corresponding to case 3 in which the polyimide sheet covers 33% of the interface (t: thickness).

Table 1   Degradation patterns for experiment and numerical simulaiton. R_d indicates the contact resisntace at the degraded area in the terminal joint.

Cases	Polyimide sheet in the experiment					Contact resistance in the numerical analysis				
	Zone A1	Zone A2	Zone B1	Zone B2	Zone B3	Zone A1	Zone A2	Zone B1	Zone B2	Zone B3
0	NO	NO	-	-	-	0	0	-	-	-
1	YES	NO	-	-	-	R_d	0	-	-	-
2	NO	YES	-	-	-	0	R_d	-	-	-
3	-	-	YES	NO	NO	-	-	R_d	0	0
4	-	-	NO	YES	NO	-	-	0	R_d	0
5	-	-	NO	NO	YES	-	-	0	0	R_d
6	-	-	YES	YES	NO	-	-	R_d	R_d	0
7	-	-	NO	YES	YES	-	-	0	R_d	R_d
8	-	-	YES	NO	YES	-	-	R_d	0	R_d

B1, B2, and B3) regions to assume some degradation patterns. Because the purpose of this study was to observe the tendency of electric potential distribution in the terminal joint with significant degradation, the smallest area of degradation was set to be 33% of the entire area of the joint interface. Table 1 shows the distribution of the polyimide sheets for nine cases (cases 0 - 8). This mockup was placed between two stainless steel plates, as shown in Fig. 5, and was compressed by tightening the bolts at 80 N/m. Copper e-probes with a diameter of 1.5 mm were then attached to the copper sleeve surface with a support jig, as shown in Fig. 5. The interval of the probes in the longitudinal direction (the x-direction) was 68 mm. The distance between two e-probes paired in the same x-direction was 14.2 mm.

A test current of 20 A was applied to the mockup to avoid significant heating in the conductor. The electric potential difference between two copper sleeves ($V_0(x)$) was then measured using pairs of two e-probes along the x-direction. V_0 (x) was measured at both RT and 77 K. The mockup was cooled by immersion in liquid nitrogen at 77 K. The DC power supply PAN35-20A (Kikusui Electronics Corp.) and a nanovolt meter 2182A (Keithley) were used for the current supply and $V(x)$ measurements, respectively. V_0 (x) was constantly measured for 30 s, and its mean value at each location ($V_{0m}(x)$) was recorded. The output voltage from the nanovolt meter without the test current was also measured as the background voltage before (V_{BGb}) and after (V_{BGa}) each measurement. Finally, $V(x) \equiv V_{0m}(x) - (V_{BGb} + V_{BGa})/2$ was evaluated for discussion.

4. Numerical Analysis

It is difficult to experimentally investigate the influence of a wide-range contact resistance on the electric potential distribution. Thus, numerical analysis was performed to assess the contact resistance dependence of the electric potential distribution. The analysis was performed using the commercial finite element analysis code Ansys Mechanical 2022 [8]. Figure 6 shows the three-

(a) Location of the e-probes

(b) Support jig for the e-probes

(c) E-probe
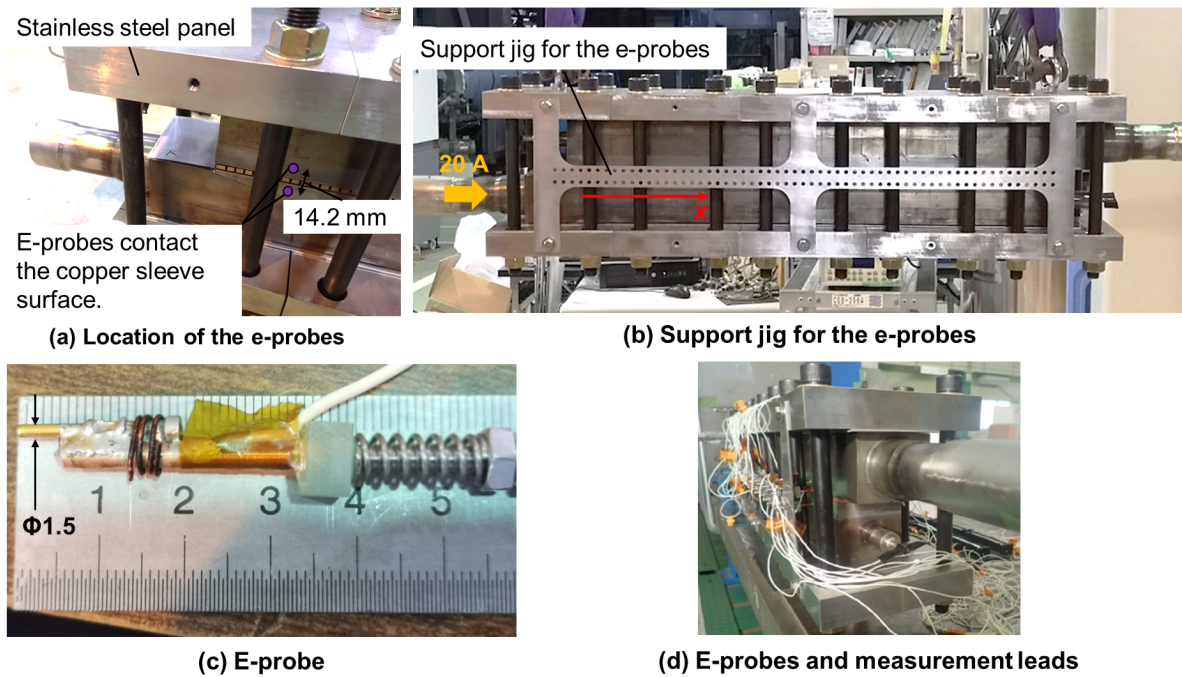
(d) E-probes and measurement leads

Fig. 5   Mockup of terminal joint for experiment; (a) location of e-probes on copper sleeve, (b) support jig for e-probes, (c) structure of e-probe, and (d) wiring of measurement leads for e-probes.
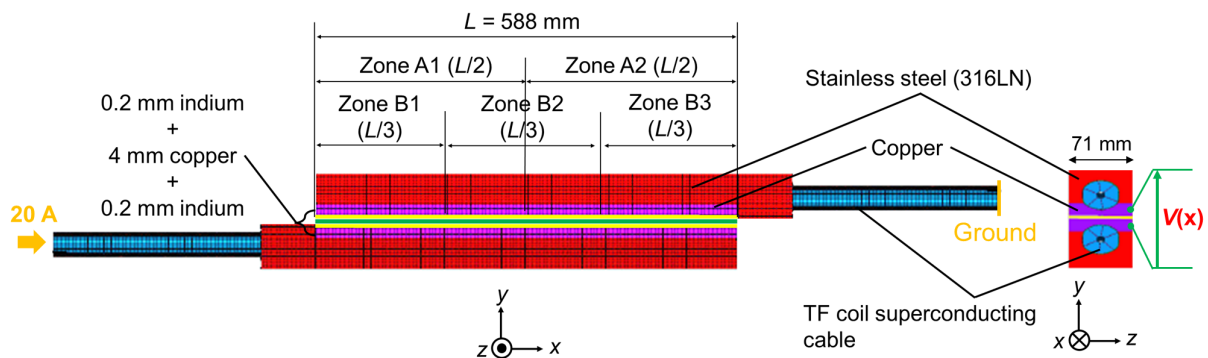

Fig. 6   Three-dimensional analytical model of the terminal joint and boundary conditions for the finite element analysis.

dimensional analytical model. The model comprises two superconducting conductors and several interface materials. The superconducting conductor comprises a stainless steel jacket, copper sleeve, and superconducting cables. There are two types of interface materials: copper shim and indium. The thicknesses of the copper shim and indium are 4 and 0.2 mm, respectively. Figure 6 also shows the boundary conditions. A test current of 20 A was applied to the cross-section of the superconducting conductor at one edge, and the electric potential was fixed to 0 V on the cross-section of the superconducting conductor at another edge. A total of 196,216 hexahedron elements were used, with the maximum element size being 5 mm × 5 mm × 5 mm and the minimum element size being 3.9 mm × 0.1 mm × 5 mm.

Similar to the experiment, nine degradation patterns in the terminal joint were assumed by locally increasing the

Table 2   Electrical resistivity used for numerical analysis.

Material	Electrical resistivity [μΩm]	
	300 K	77 K
Stainless steel 316LN [9]	7.69×10^{-1}	5.68×10^{-1}
Copper (RRR = 100) [10]	1.70×10^{-2}	2.10×10^{-3}
Indium [11]	8.85×10^{-2}	1.67×10^{-2}
Superconducting cable [5]	3.85×10^{-2}	2.60×10^{-3}

interface resistance between the indium and copper shim (R_d), as shown in Table 1. R_d was set to 5.0×10^{-9} - 10^9 Ωmm². 300 K (RT) and 77 K were assumed as the two operating temperatures. The influence of temperature was

considered in the temperature dependence of the electrical resistivity.

Table 2 shows the resistivity values of the materials assumed in the analysis, which were obtained from [5, 9–11]. Notably, the influence of the contact resistance among the superconducting wires and between the superconducting wires and stainless steel jacket is considered in the analysis of the resistivity of the superconducting cable.

5. Results and Discussion
5.1 Electric potential distribution for different degradation patterns

The electric potential distributions between the e-probes on the upper and lower copper sleeves ($V(x)$) in the experiment and numerical analysis at $R_d = 10^9 \, \Omega mm^2$ are compared. Figures 7 and 8 show examples of $V(x)$ in (a) case 0 (no degradation is considered), (b) case 4 (degradation is in the 33% central area), and (c) case 7 (degradation is in the 66% downstream area) at RT and 77 K. Note that the "downstream area" represents the area near the grounded surface. The degraded area is highlighted in orange in the figures.

The location of the peak of $V(x)$ corresponds to the center of the degraded area. The peak value of $V(x)$, which is the maximum $|V(x)|$ (V_{max}), varies in accordance with the degradation conditions. Table 3 shows V_{max} with different degradation patterns at RT and 77 K. Here, the nanovolt meter outputs voltages up to 10 nV. The table also shows the background noise ($= |V_{BGb} - V_{BGa}|$) in brackets. The background noise at 77 K shows the same level or a larger value than that at RT, except for case 0. This is because of the boiling of liquid nitrogen during the measurement. When there is degradation in the contact resistance (cases 1 - 8), V_{max} becomes 4 - 80 μV and 2 - 70 μV in the experiment and numerical analysis, respectively, and these results agree well.

Although the degraded area in this study (33% - 66% of the joint interface) is smaller than that in the case of the DPJ (80% of the joint interface) [3], the largest (smallest) V_{max} in this study is almost the same as (larger than) the V_{max} in the DPJ. This is because of the difference in the current path between the DPJ and terminal joint, as illustrated in Fig. 2. The current decreases in the area near the end of the joint in the DPJ [3], whereas it flows over the entire area in the terminal joint. Thus, $V(x)$ is more sensitive to nonuniform degradation in the terminal joint than in the DPJ.
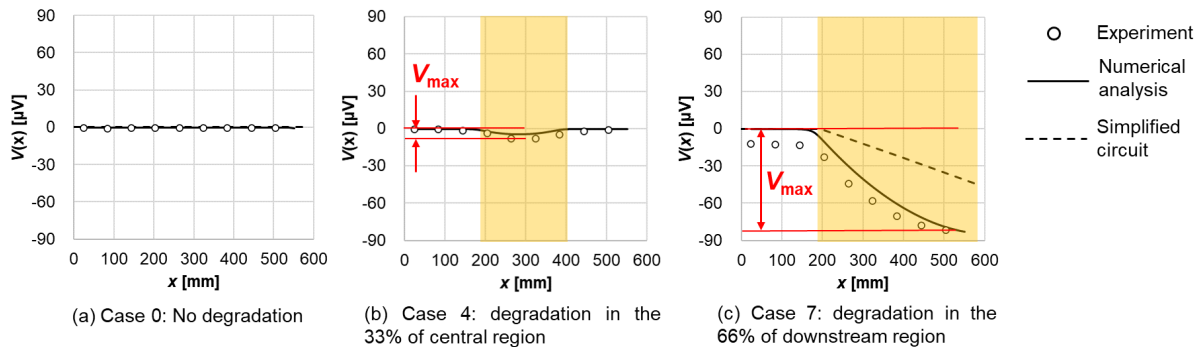

Fig. 7 The values of $V(x)$ obtained from experiment (open circle), numerical analysis (solid curve); (a) case 0, (b) case 4, and (c) case 7 at RT. $V(x)$ denotes the voltage difference between copper sleeves, and x represents the distance from the edge of the joint interface. The values of $V(x)$ estimated with simplified circuit in (a) case 0 and (c) case 7 are also plotted (dotted curve).
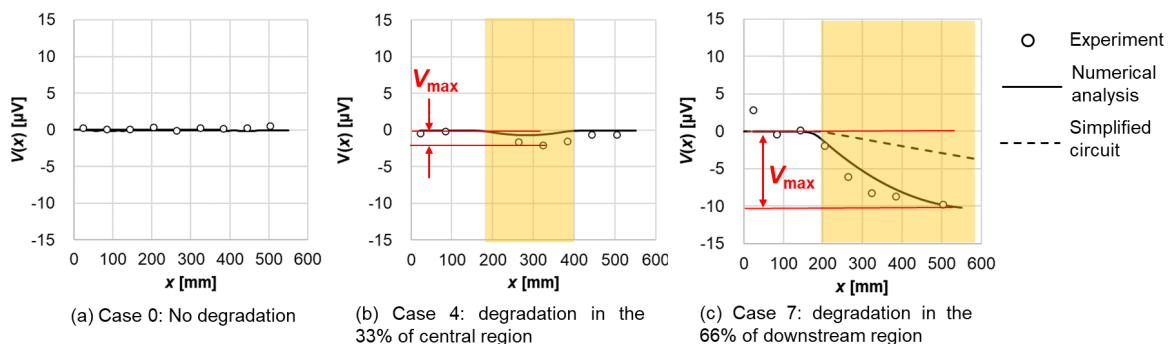

Fig. 8 The values of $V(x)$ obtained from experiment (open circle), numerical analysis (solid curve); (a) case 0, (b) case 4, and (c) case 7 at 77 K. $V(x)$ denotes the voltage difference between copper sleeves, and x represents the distance from the edge of the joint interface. The values of $V(x)$ estimated with simplified circuit in (a) case 0 and (c) case 7 are also plotted (dotted curve).

Table 3 V_{max} in the experiment and numerical analysis, where the values in brackets are the background noise.

Cases	V_{max} in the experiment [μV]		V_{max} in the numerical analysis [μV]	
	RT	77 K	RT	77 K
0	0.47 (0.96)	0.27 (0.58)	0.34	0.04
1	50.1 (0.14)	5.01 (1.04)	51.3	5.7
2	37.2 (0.64)	5.84 (0.93)	46.3	6.02
3	17.9 (1.01)	3.97 (1.34)	23.2	2.61
4	7.84 (0.60)	2.1 (0.58)	4.86	0.69
5	24.6 (0.45)	2.53 (1.75)	26.4	2.89
6	63.9 (0.43)	10.6 (0.39)	75.5	9.77
7	81.4 (0.16)	9.79 (1.33)	82.9	10.2
8	24.9 (0.91)	5.03 (1.08)	23.4	2.7

Fig. 9   Simplified circuit model of terminal joint in case 0; (a) major current paths, and (b) distribution of current at each branch (green color) and electric potential at each node (blue color).

Fig. 10   Simplified circuit model of terminal joint in case 7; (a) major current paths, and (b) distribution of current at each branch (green color) and electric potential at each node (blue color).

In the cases of the terminal joint with degradation, both experimental and analysis results at RT and 77 K show the smallest V_{max} in case 4. The largest V_{max} was observed in cases 6 and 7 in the experiment and numerical analysis, respectively. This difference is caused by the background noise of the measurement at 77 K in the experiment, which is 0.39 - 1.75 μV, as shown in Table 3. Although the V_{max} in case 7 is larger than that in case 6 in the numerical analysis, the difference is only ~0.2 μV. Thus, this difference is practically negligible considering the background noise at 77 K.

The causes of the variation of V_{max} values can be quantitatively understood from the current distribution in the terminal joint with a simplified circuit analysis. Figures 9 and 10 show the one-dimensional simplified electrical circuit of the terminal joint in cases 0 and 7, respectively. Note that continuous current distribution inside each 196-mm region is not considered in this circuit. Only the resistace of the joint box (bulk resisatnce) in the horizontal direction are shown since it would be larger than that in the vertical direction and the resistance fo the inserted materials, such as copper and indium. R [Ω] denotes the equivalent resistance of the joint box. Figures 9 and 10 show the current and electric potential distribution in cases 0 and 7, respectively. In Fig. 10, two major current paths, A and B, are illustrated for the upper and lower joint boxes, respectively. The current and electric potential were estimated on the basis of the simplified circuit. In case 4, the current distribution showing the small |V(x)| would be similar
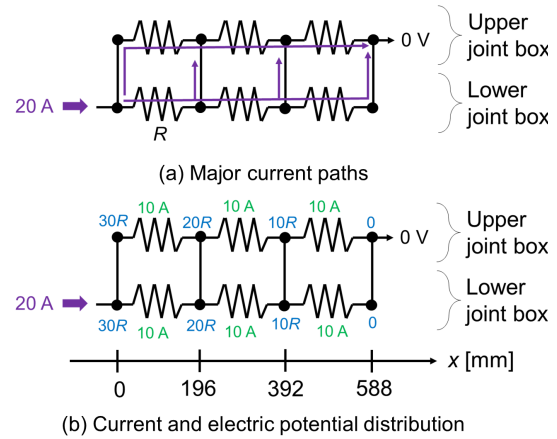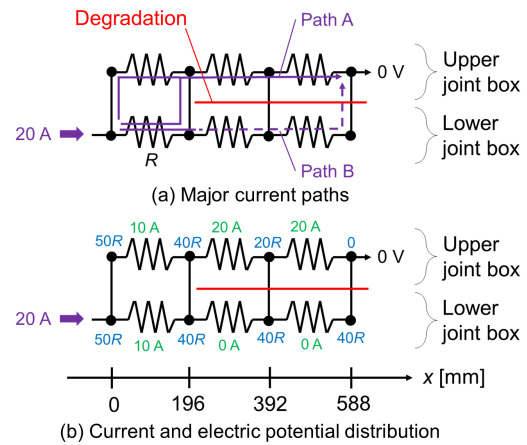
to that in case 0, except for the local current distribution around the degradation. Conversely, in case 7, the equivalent resistances of current paths A and B are almost infinite and $3R$, respectively. Thus, the smaller current flows into the upper copper sleeve, resulting in a large |V(x)| of $40R$ [V] (= |0 − 40R|) at $x = 588$ mm. $V(x)$ estimated using the simplified circuit model ($V_s(x)$) is also plotted in Figs. 7 and 8. R was assumed to be 1.14 μΩ at RT and 0.094 μΩ at 77 K. |$V_s(x)$| is lower than |$V(x)$| in the experiment (|$V_{exp}(x)$|) and numerical analysis (|$V_{num}(x)$|) in case 7 because the resistance between the superconducting filaments and the copper sleeve is not considered in the simplified circuit model. However, $V_s(x)$ quantitively agrees with $V_{exp}(x)$ and $V_{num}(x)$. Thus, the discussion above is reasonable, and the bulk resistance through the major current path is considered a key parameter for the relationship

between $V(x)$ and the degraded location at >77 K.

5.2 Dependence of contact resistance on the electric potential profile

Considering the sensitivity of signals to degradation, it is important to focus on not only the value of V_{max} but also on the extent to which V_{max} changes with different degradation patterns. Thus, the parameter α is defined as $\alpha \equiv$ the largest V_{max} (case 7) / the smallest V_{max} (case 4) as an indicator of the effect of temperature on the proposed method. Notably, cases 7 and 4 exhibited large and small V_{max} values, as shown in Table 3. Thus, α represents how much the temperature changes the difference in $V(x)$ with different degradation patterns. The α values obtained in the numerical analysis at 300 K and 77 K are compared. Consequently, α is 13.9 at both 300 K and 77 K in the numerical analysis. Thus, there appears to be no advantage in cooling the joint in the case of $R_d = 10^9 \, \Omega mm^2$. However, the α value at 77 K may be larger than that at 300 K with a smaller R_d if R_d is sufficiently smaller than the bulk resistance in the terminal joint. Figure 11 summarizes α and the difference in V_{max} between cases 4 and 7 (ΔV_{max}) when R_d is 5.0×10^{-9} - $10^9 \, \Omega mm^2$. The α value at 77 K is larger than that at 300 K when R_d is $< 5.0 \times 10^{-4} \, \Omega mm^2$. This larger α value at 77 K helps to distinguish the degradation patterns. Given the level of background noise, $1 \, \mu V$ would be the limit, and this method would fail when R_d is $< 1.0 \times 10^{-5} \, \Omega mm^2$. Notably, detectable R_d can be increased by increasing the test current as much as possible. Considering the minimum detectable R_d, cooling of the terminal joint is effective only when $1.0 \times 10^{-5} \, \Omega mm^2 < R_d < 5.0 \times 10^{-4} \, \Omega mm^2$ in terms of α. Moreover, ΔV_{max} at 300 K is several times larger than that at 77 K. Thus, the proposed method works at RT without cooling the terminal joint when the degraded area is more than 33% of the joint interface. Degradation of 33% of the joint interface with R_d of $1.0 \times 10^{-5} \, \Omega mm^2$ corresponds to 0.73 nΩ (= $1.0 \times 10^{-5} \, \Omega mm^2$/(588 mm × 71 mm

× 33%)), which is less than the criteria for an overall resistance of 3 nΩ at 4 K [1]. Thus, this method is useful to check major distributed degradation, such as the air gap due to the misalignment of the joint boxes at any step before cooling or even at the training of the joint assembly.

6. Conclusion

In this study, we proposed the use of the e-probe method for the inspection of an ITER toroidal field terminal joint, and its applicable conditions and characteristics of voltage signals were numerically and experimentally investigated. The assumed degradation is uniform in the width direction and distributed in the longitudinal direction, which could occur because of the imbalanced compression of the joint during the TFC-feeder assembly. The highlights are as follows:

- The experimental and analysis results indicate that 2.1 - 81.4 μV and 0.7 - 82.9 μV are detectable when R_d in more than 33% of the joint interface is $10^9 \, \Omega mm^2$. The difference in the voltage signal above 77 K is primarily caused by the bulk resistance of the major current paths.

- The parameter α is defined to evaluate the sensitivity of the voltage signal to degradation. The value of α at 77 K is larger than that at RT when R_d is $< 5.0 \times 10^{-4} \, \Omega mm^2$. Considering the limitation of detectable contact resistance in the degraded area, where R_d is $< 1.0 \times 10^{-5} \, \Omega mm^2$, cooling of the terminal joint is effective when $1.0 \times 10^{-5} \, \Omega mm^2 < R_d < 5.0 \times 10^{-4} \, \Omega mm^2$. However, the range of R_d in which cooling is effective is small, and ΔV_{max} at RT is still several times larger than that at 77 K. Thus, the proposed method works at RT without cooling to detect a degraded area exceeding 33% of the joint interface.

These findings show the limitations and applicability of the proposed method and will be useful information for the design of an inspection procedure of the ITER toroidal field terminal joint during the assembly phase.
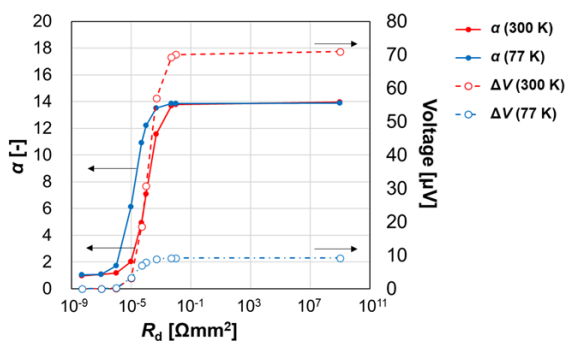
Fig. 11 Relationship between α and R_d (solid line), and between V_{max} and R_d (dotted line) at 300 K and 77 K where α is defined as the largest V_{max} (case 7) / the smallest V_{max} (case 4).

[1] Y. Ilyin *et al.*, "Design and Qualification of Joints for ITER Magnet Busbar System", IEEE Trans. Appl. Supercond. **26**, 4800905 (2016).

[2] Y. Ilyin *et al.*, "Qualification Program of Lap Joints for ITER Coils", IEEE Trans. Appl. Supercond. **28**, 4201306 (2018).

[3] H. Kajitani *et al.*, "New Inspection Method of Soldering Region at Room Temperature for ITER TF Termination", IEEE Trans. Appl. Supercond. **29**, 4200604 (2019).

[4] H. Kajitani *et al.*, "Results of All ITER TF Full-Size Joint Sample Tests in Japan", IEEE Trans. Appl. Supercond. **31**, 4201905 (2021).

[5] H. Kajitani *et al.*, "Evaluation of ITER TF Coil Joint Performance", IEEE Trans. Appl. Supercond, **25**, 4202204 (2015).

[6] E.W. Collings, "Anomalous electrical resistivity, bcc phase stability, and superconductivity in titanium-vanadium alloys", Phys. Rev. B **9**, 3989 (1974).

[7] Z. Ren *et al.*, "Evolution of T^2 resistivity and superconductivity in Nb_3Sn under pressure", Phys. Rev. B **95**, 184503

(2017).

[8] Ansys® Mechanical, Release 18.2

[9] A.F. Clark *et al.*, "Electrical resistivity of some engineering alloys at low temperatures", Cryogenics **10**, 295 (1970).

[10] J.G. Hust *et al.*, "Standard Reference Materials for Thermal Conductivity and Electrical Resistivity", In: Klemens P.G., Chu T.K. (eds) Thermal Conductivity 14 (Springer, Boston, MA., 1976).

[11] G.K. White *et al.*, "Metals: Electronic Transport Phenomena", In: J. Bass (eds) (Springer, Boston, MA., 1957).